Research Article

Received: 15 December 2015 Revised: 1 March 2016 Accepted article published: 8 April 2016 Published online in Wiley Online Library: 12 May 2016

(wileyonlinelibrary.com) DOI 10.1002/pi.5127

Influence of incorporation of starch nanoparticles in PBAT/TPS composite films

Paula González Seligra,[a] Lídia Eloy Moura,[b] Lucia Famá,[a†] Janice Izabel Druzian[b†] and Silvia Goyanes[a*]

Abstract

Films of PBAT/TPS (poly(butylene adipate-*co*-terephthalate)/thermoplastic starch) (starch plasticized with glycerol containing citric and stearic acids) without and with 0.6 wt% starch nanoparticles were produced by extrusion. The presence of nanoparticles during the extrusion process led to a higher degree of starch gelatinization improving starch compatibility with PBAT. Nanoparticles modified the interaction between the different components of the PBAT/TPS composite. The hydroxyl groups of the starch nanoparticles interacted with starch amylose by means of hydrogen bonds. In addition, nanoparticles modified the structure of the PBAT rigid segment (BT): a shift of T_m of BT toward lower temperatures and a slight shift of the relaxation of the BT segment to higher temperatures were observed. The incorporation of nanoparticles also had a reinforcing effect on the PBAT/TPS matrix. The composite presented slight increases of Young's modulus (E) and stress at break (σ_b) without affecting the strain at break (ε_b). The rate of biodegradability was improved with the use of starch nanoparticles. The composite showed faster deterioration than the matrix, showing the first changes in its tonality and breakdowns at only 6 days of burial in compost.

Keywords: PBAT; TPS; starch nanoparticles; thermal properties; biodegradability

INTRODUCTION

The worldwide interest in biodegradable polymers has accelerated in recent years due to an increased concern about environmental issues, with regard to persistent plastic wastes and air pollution.[1–4] Poly(butylene adipate-*co*-terephthalate) (PBAT), an aromatic–aliphatic copolyester, is a biodegradable polymer from petrochemical resources with processing conditions and mechanical properties similar to those of polyethylene.[5,6] However, although PBAT is a promising material for the production of environmentally friendly biodegradable polymers, it presents two important disadvantages: its higher cost and slower biodegradability. The PBAT degradation time, about 4 months, is similar to that of poly(lactic acid)[7] and higher than that of thermoplastic starch.[8] In order to reduce the cost of the final product and accelerate its degradation, to make it more competitive, several researchers have studied PBAT blends with other biodegradable polymers.[9–11]

Starch is a completely biodegradable polymer, non-abrasive, readily available and inexpensive, and can be obtained from renewable sources.[12–14] In this sense, starch can be an alternative to PBAT blends, as it can reduce the cost of the final product as well as improve its biodegradation characteristics, making the blend very promising compared to PBAT materials.[15] According to Kalambur and Rizvi,[16] the amount of starch that can form blends with polyesters, with such important properties as poor deterioration, is typically 25%–30%. In particular, different authors have evaluated the effect of different concentrations of starch in mixtures with PBAT, showing that the use of 30% starch leads to a better dispersion and smaller particle size of thermoplastic starch (TPS) in the PBAT matrix.[17,18]

Generally, in PBAT blends, starch has been used in the form of TPS. Fluid TPS is obtained from the disruption of the native starch granules when these are submitted to mechanical/thermal treatment in the presence of plasticizers.[19]

Unfortunately, the hydrophilicity of starch and the hydrophobicity of PBAT led to a poor interfacial adhesion between them. To improve the deficient interfacial adhesion between the two components, compatibilizers were used, citric acid being the most employed.[20,21] Carboxylic acids, such as citric and stearic acids, have a polar group (COOH) that can react with the hydroxyl groups of starch through secondary bond forces, decreasing starch hydrophilicity and increasing the compatibility with PBAT.[20,22] Notwithstanding, natural compatibilizers such as citric acid do not always lead to better results.[20] Another alternative to improve the compatibility between TPS and PBAT, which is not much explored in the literature, is the addition of nanofillers.[15,17,23]

The most frequent nanoparticle used in the literature is the hydrophilic filler.[17,23] This is because hydrophilic nanoparticles present more OH that can form hydrogen bonds with the hydrophilic polymer of the blends (starch),[19,24,25] improving

* *Correspondence to: S Goyanes, LP & MC, Dep. de Física – IFIBA (CONICET), FCEyN, UBA, Ciudad Universitaria (1428), CABA, Argentina. E-mail: sgoyanes@gmail.com*

† *These authors contributed equally to this work.*

a *LP & MC, Dep. de Física – IFIBA (CONICET), FCEyN, UBA, Ciudad Universitaria (1428), CABA, Argentina*

b *Department of Bromatological Analysis, College of Pharmacy, Federal University of Bahia, Barão of Geremoabo Street, Ondina, Salvador, Bahia 40171-970, Brazil*

the dispersion of the filler and thus the mechanical, thermal and biodegradability properties.[15,17] The effect of hydrophobic nanofillers was also evaluated in PBAT nanocomposites. Mohanty and Nayak[26] demonstrated that hydrophobic nanoclays improved the thermal stability of PBAT nanocomposites due to their ability to act as a heat barrier.

It is well known that starch nanoparticles are hydrophilic fillers.[24,26] Angellier *et al.*[24] showed that starch nanoparticles are characterized by presenting an OH-rich surface, because they exhibit a polar component as high as the dispersive one. This particularity makes the nanoparticles very compatible with the PBAT/starch blend.

Acid hydrolysis is the typical way to generate starch nanocrystals.[25,27,28] However, the acid hydrolysis method is not appropriate for industrial applications due to its negative environmental impact. Gamma irradiation emerges as a novel method for producing starch nanoparticles since it generates free radicals on starch molecules that are capable of hydrolysing chemical bonds and thereby cleaving the large molecules of starch into smaller fragments of dextrin.[29] Compared with acid hydrolysis, gamma irradiation treatment is easy, immediate and convenient as it may allow higher mass production of the starch nanoparticles with low costs, using a simple and scalable methodology.[30]

To the best of our knowledge, the effect of the incorporation of starch nanoparticles in PBAT/TPS blends has not been studied.

The aim of this work was to study the influence of the addition of starch nanoparticles into a PBAT/TPS blend-based film, through the determination of its effect on the polymer compatibility, the thermal and mechanical properties and the biodegradability of the material.

EXPERIMENTAL

Materials

Cassava starch was provided by Cargill Agrícola S.A. (Porto Ferreira, Brazil). PBAT (Ecoflex®S BX 7025) was supplied by Basf, Ludwigshafen, Germany. Glycerol (Synth®, Diadema, Brazil) and stearic and citric acids (Vetec, Duque de Caxias, Brazil) were of analytical grade. Native waxy starch (99 wt% amylopectin) was provided by Roquette S.A., Lestrem, France.

Starch nanoparticle production

Starch nanoparticles were produced using gamma radiation according to Lamanna *et al.*[30] Starch stable dispersions were prepared by mixing 5 g of waxy starch in 500 mL of boiling water. Then, samples were irradiated with 20 kGy using a ^{60}Co gamma-ray source in the facilities of the Ezeiza Atomic Centre, Argentina.

Preparation of the films

PBAT/TPS (70:30) films were obtained by the extrusion process using a laboratory twin-screw extruder (model AX16DR, AX Plásticos, São Paulo, Brazil) with a screw diameter (*D*) of 16 mm and length to diameter ratio (*L*/*D*) of 40*D*. Glycerol was used as plasticizer, and citric and stearic acids as compatibilizers.

The films were prepared following three steps, according to Silva *et al.*[31] The first involves the preparation of TPS with starch nanoparticles. A solution containing glycerol (7.5 wt%), compatibilizing citric acid (0.6 wt%) and stearic acid (0.3 wt%), with or without starch nanoparticles, was mixed with starch. The concentration of nanoparticles used was 0.6 wt% of the matrix. The mixture was dried at 50 °C for 24 h, gently homogenized using a manual mixer device for 5 min and passed through a sieve mesh (9 mm) (Bertel, São Paulo , Brazil).

In the second stage, PBAT/TPS blends in the ratio 70:30 were prepared. Pellets were obtained by extruding from the dry mixtures using a twin-screw extruder. The screw speed was 39 rpm and the barrel zone temperature profile was set at 80/90/100/105/105/105/110/110°C from the feeding zone (zone 1) to the die zone (zone 8). The extruded strands were obtained using a pellet die (3 mm in diameter) and cut into pellets with a cutting device.

In the third and last stage, the pellets were processed to obtain the final material in the form of films, so a controlled temperature film planar die was connected to the barrel exit. The pellets were loaded into the extruder (feed speed 35 rpm) at a screw speed of 50 rpm and temperature profile of 100/120/125/130/135/140/140/140 °C (zones 1–8). The thickness of both matrix and composite was 0.40 ± 0.02 mm.

Characterization techniques

The developed films were conditioned for 15 days, at 25 °C, over a saturated solution of NaBr (relative humidity *ca* 56%) before being characterized.

Scanning electron microscopy (SEM)

The morphology of the starch nanoparticles and the cryogenic fracture surface of the developed films (matrix and composite) was tested by field emission SEM (FE-SEM) using a Zeiss DSM982 Gemini with a field emission gun equipment.

Fourier transform infrared spectroscopy (ATR/FTIR)

The infrared spectra of the starch nanoparticles and films were recorded on a Nicolet Nexus (Madison, WI, USA) Fourier transform infrared spectrometer, using the attenuated total reflectance (ATR) accessory. Measurements were obtained as the average of 32 scans, in the range from 4000 cm^{-1} to 600 cm^{-1}, with a resolution of 2 cm^{-1}.

Thermal characterization

A simultaneous thermogravimetric/differential thermal analyser (TGA/DTA DTG-60 Shimadzu instrument, Kyoto, Japan) was used to evaluate the thermal properties of the films. Approximately 10 mg of each sample was subjected to heating from 30 °C to 500 °C at a rate of 10 °C min^{-1} in a dry nitrogen atmosphere. The flow rate of nitrogen was 30 mL min^{-1}. Thermal properties were evaluated from the curves of both TGA and DTA.

Differential scanning calorimetry (DSC)

DSC analyses were carried out with DSC 4000 Perkin Elmer (MA, USA) equipment, with a thermal cooling accessory. Approximately 10 mg of samples were weighed and placed in aluminium sample pans, which were immediately sealed. An empty sample pan was used as reference. Film samples were heated from −80 °C to 200 °C under a nitrogen atmosphere at a heating rate of 10 °C min^{-1}. The transition temperatures were determined from the thermogram curves.

Mechanical properties

Mechanical characterizations (uniaxial tensile and dynamic tests) of the developed films were performed. Uniaxial tensile tests were carried out in an Instron dynamometer at a crosshead speed

of 5 mm min^{-1} at room temperature, following ASTM D882-02 (2002) standard recommendation.[32] From stress–strain curves, Young's modulus (E), the stress at break (σ_u) and the strain at break (ε_b) were determined. The dimensions of the samples for this assay were 10.0 mm × 5.0 mm × 0.40 mm (length, width and thickness). The values reported are the average of at least 10 measurements.

The dynamic mechanical properties of the developed films were studied using a dynamic mechanical thermal analyser (DMTA IV, Rheometric Scientific, USA) in the rectangular tension mode at 1 Hz, in the temperature range between −60 °C and 120 °C, at a heating rate of 2 °C min^{-1}. The cyclic strain value was 0.04% to assure that the mechanical response of the samples was within the linear viscoelastic range. The dimensions of the samples were 20.0 mm × 5.0 mm × 0.40 mm (length, width and thickness). Three replicates were tested for each system.

Contact angle

Contact angle analyses were carried out using a microscope MicroView (USB Digital Microscope) coupled with image analysis software (Analysis Software 220x 2.0 MP) on an OCA 20 goniometer (Data Physics, USA). A drop of water of *ca* 2 µL was deposited on the surface of each film. The methodology to calculate the contact angle (θ) was based on the processing of images by determining the angle formed by the intersection of the liquid–solid interface (drop of water – surface of the film) and the liquid – vapour interface (tangent to the boundary of the drop).[33] The average of eight measurements was reported.

Moisture content

The moisture content of the films was determined using the standard methods of analysis of the Association of Official Analytical Chemists.[34] Pieces of each sample (*ca* 0.5 g) were dried in an oven at 100 °C for 24 h. The percentage of moisture content (MC) was calculated as follows:

$$\mathrm{MC}\ (\%) = \frac{m_w - m_d}{m_d} \times 100 \qquad (1)$$

where m_w is the mass of the wet sample and m_d is the mass of the dried sample. The reported results represent the average of five samples in each case.

Biodegradation of the films in vegetable compost

The samples were cut into pieces of 2 cm × 2 cm. The vegetable compost, which was used as soil, was sifted to remove large clumps and poured into plastic trays up to a thickness of about 6 cm. Samples were buried below 4 cm of soil, and the plastic trays were under ambient temperature (*ca* 25 °C) and humidity conditions (70% – 80%). Water was sprayed twice a day to sustain the moisture of the compost. The films were removed at different times and dried in a vacuum oven at 50 °C for 24 h.

RESULTS AND DISCUSSION

Morphological characterization

An FE-SEM micrograph of the nanoparticles used is shown in Fig. 1. Particles with a diameter below 100 nm were obtained, most of them being around 50 nm. Some agglomerates are observed in the micrograph due to the large number of OH groups on their surface.[30]

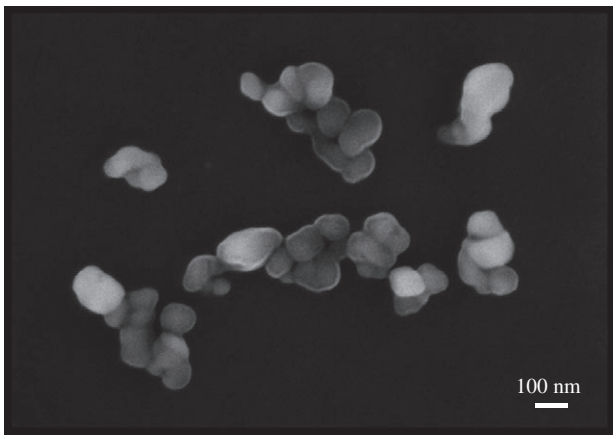

Figure 1. FE-SEM micrograph of starch nanoparticles produced by gamma radiation.

Figure 2 shows micrographs of the cryogenic fractured surfaces of the developed films (matrix and composite). Both samples showed starch particles distributed in the PBAT matrix. Films without nanoparticles presented starch grains in the range 2–10 µm and some broken starch grains, in accordance with the literature.[23] Phase separation, clearly observed in the micrograph, is a consequence of the different polarities of starch (hydrophilic) and PBAT (hydrophobic). The broken grains suggest that the starch gelatinization process during the extrusion was incomplete. According to the literature, it is not easy to completely break starch grains in the presence of PBAT.[35] While it is known that the use of compatibilizers reduces the size of the starch phase in PBAT, phase separation between the polymers remains frequent.[6,18,36] Comparing the cryogenic fracture surface micrographs of the two materials (Figs 1(b) – (d)), a higher amount of broken starch grains can be seen in the composite. Despite the decrease of whole starch grains, the presence of broken grains indicates that the nanocomposite was not completely gelatinized. Consequently, a co-continuous thermoplastic phase was not observed. The appearance of a higher amount of broken starch grains and the decrease of grain number per unit area suggest that the presence of nanoparticles helped the starch gelatinization process, since it occurs for grain disruption processes.

Fourier transform infrared spectroscopy (ATR/FTIR)

ATR/FTIR spectra of the matrix, composite and starch nanoparticles are given in Fig. 3. The spectra corresponding to both films showed the following bands: around 3300 cm^{-1}, which corresponds to the stretching of OH groups;[37] two between 2950 cm^{-1} and 2850 cm^{-1} that are associated with asymmetric and symmetric C – H stretching of the methylene group (–CH_2–), respectively;[38] at *ca* 1715 cm^{-1}, due to the stretching of carbonyl (C = O) in the ester linkage; at *ca* 1263 cm^{-1} , associated with C – O groups; at 1020 cm^{-1}, with stretching due to the presence of substituted benzene rings; and a peak at 720 cm^{-1}, representing adjacent methylene groups (–CH_2–).[38]

In order to show the effect of the incorporation of nanoparticles in the matrix, an amplification of the zone around 2900 cm^{-1} is shown (Fig. 3(B)). The matrix presented the bands associated with asymmetric and symmetric C – H stretching of CH_2 at *ca* 2917 cm^{-1} and 2850 cm^{-1}, respectively. In the composite, these bands are shifted to a higher wavenumber (around 2948 cm^{-1} and 2884 cm^{-1}) and widened. Taking into account the nanoparticle

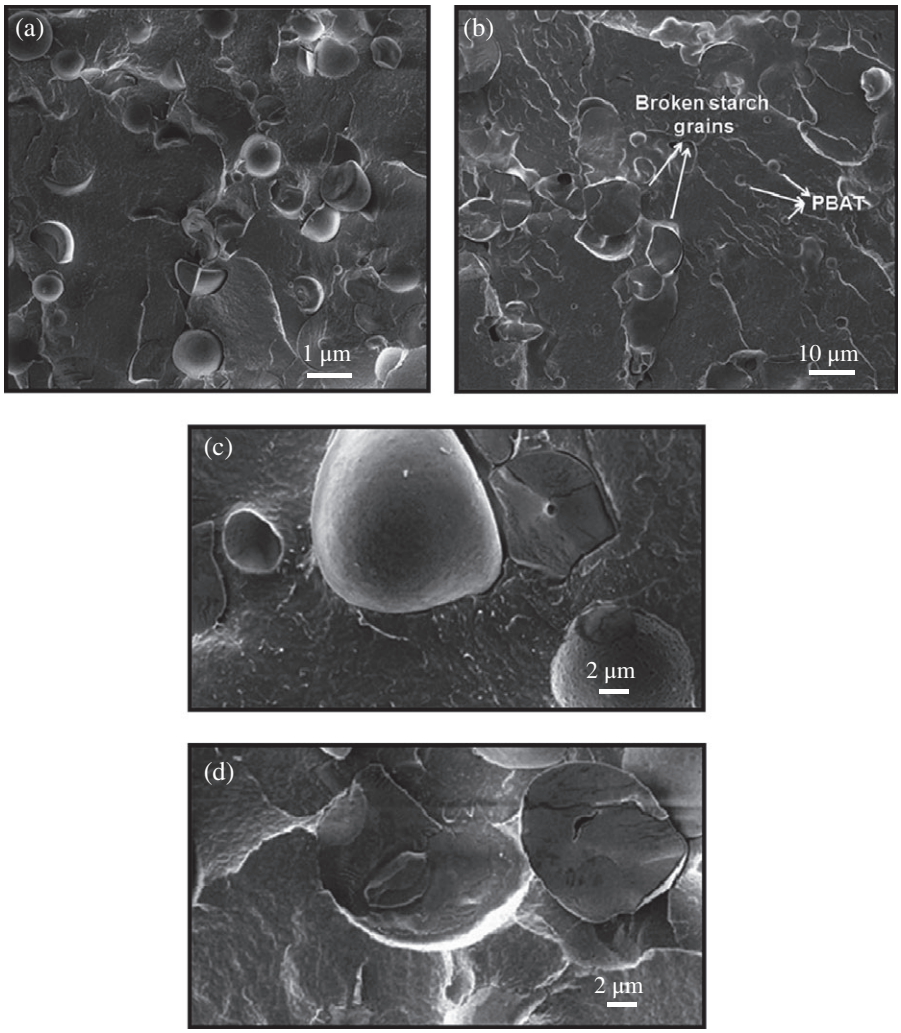

Figure 2. FE-SEM micrograph of the cryogenic fracture surface of (a), (c) matrix and (b), (d) composite at different magnifications.

spectrum in that zone, where two wide bands are presented at a similar wavenumber in relation to the composite, it is possible to conclude that the nanoparticles interacted well with the PBAT/starch matrix during the extrusion process.

Differential thermal analysis (DTA)

The DTA curves of the films (matrix and composite) are shown in Fig. 4. The DTA results show various processes associated with gelatinization of starch, and starch and PBAT degradation. The starch gelatinization occurs because, in both films, starch grains and water are sufficient to make that process take place.

In Fig. 4(a), it can be seen that the addition of nanoparticles shifts the peak temperature of the gelatinization process to lower temperatures. This result is consistent with those obtained by SEM, which showed an increase in the number of broken grains in the composite, and therefore less energy is needed to complete the gelatinization process.

DTA curves of the films in the temperature range corresponding to the degradation of the materials are shown in Fig. 4(b). Both materials present three endothermic peaks. In the matrix, they are around 306 °C, 323 °C and 405 °C, related to the thermal degradation of amylose, amylopectin[15] and PBAT,[39] respectively. The incorporation of starch nanoparticles did not affect PBAT degradation. Nonetheless, the amylose degradation temperature was shifted towards higher temperatures (*ca* 314 °C) in the presence of nanoparticles, demonstrating interaction only with starch, preferentially with amylose, delaying its degradation.

Thermogravimetric analysis (TGA)

The thermal stability of the films is depicted in Fig. 5. Thermograms show three step degradation processes. The initial mass decrease in the range 100–270 °C corresponds to water loss and degradation of carbonyl groups and plasticizers. The composite presented slightly higher mass loss in this zone, possibly due to the greater number of OH groups introduced by the nanoparticles and the increase in the number of carbonyl groups as observed in the FTIR spectra. This result is also consistent with the higher moisture content obtained in the composite material (Table 1). The second degradation process (280–340 °C) corresponds to starch decomposition,[40] and the third mass loss, in the range 355–440 °C, is related to PBAT decomposition.[20] Similar to what is observed in the DTA results, the addition of nanoparticles does not appear to significantly modify PBAT degradation.

Finally, it is important to note that the TGA results indicate that both matrix and composite films are thermally stable up to temperatures around 280 °C.

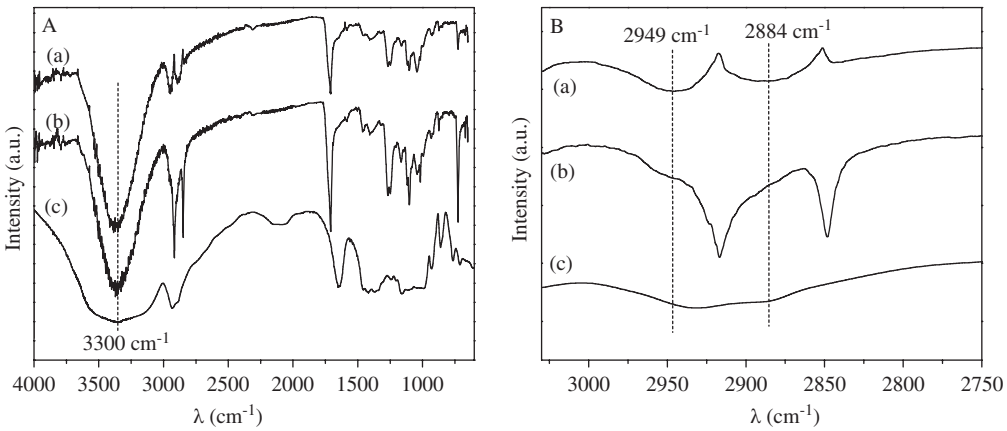

Figure 3. ATR/FTIR spectra of composite (curve (a)), matrix (curve (b)) and nanoparticles (curve (c)): (A) in the range from 4000 cm^{-1} to 600 cm^{-1} and (B) in the range from 3030 cm^{-1} to 2750 cm^{-1}.

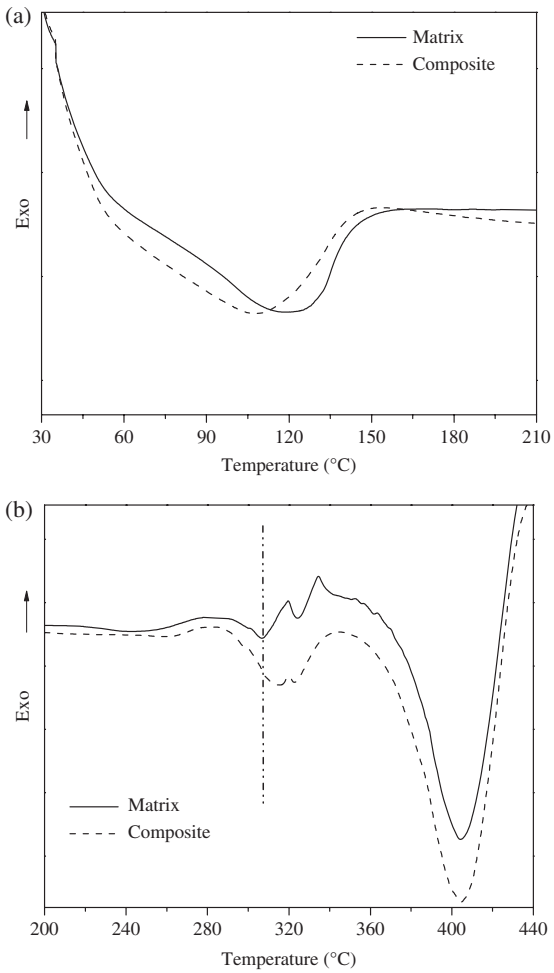

Figure 4. Differential thermal analysis for matrix and composite films: (a) between 30 °C and 210 °C and (b) from 200 °C to 440 °C.

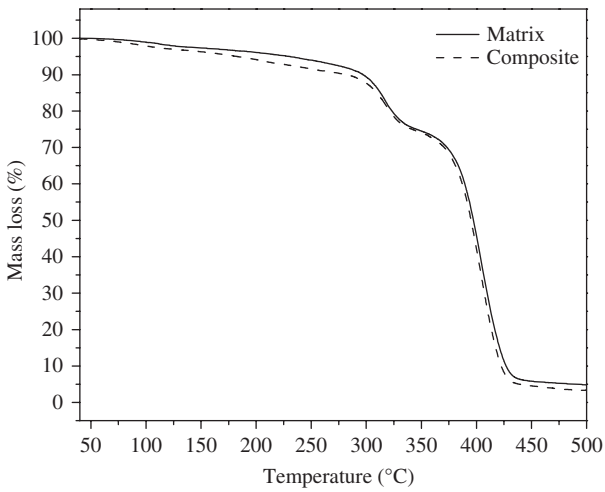

Figure 5. Thermogravimetric analysis of matrix and composite.

Table 1. Moisture content (MC) and contact angle (θ) of the developed films

	MC (%)	θ (°)
Matrix	10.0 ± 0.3	72.6 ± 1.4
Composite	12.1 ± 0.2	57.4 ± 1.8

Differential scanning calorimetry (DSC)

DSC curves of matrix and nanocomposite are shown in Fig. 6. Three transitions are observed: the first around −34 °C, another at *ca* 51 °C (both at similar temperatures in the case of matrix or composites) and the last at *ca* 143 °C for the matrix and *ca* 117 °C for the composite.

In order to understand these results, it is necessary to keep in mind the chemical structure of PBAT (Fig. 7). PBAT can be described by two repeat units: a rigid butylene terephthalate (BT) segment and a soft butylene adipate (BA) segment. Virgin PBAT presents two glass transition temperatures (T_g), one related to the motion of the flexible segment (BA) at around −20 °C and another, at *ca* 62 °C, which corresponds to the relaxation of the rigid segment (BT).[17] This last relaxation, in general, is not possible to detect by DSC. In PBAT/TPS blends, the glass transition related to the motion of BA was observed around −39 °C.[36] Then, the peak around −34 °C, observed in the thermograms of both films (Fig. 6), corresponds to the BA segment T_g of the PBAT/TPS blend. The similarity of the T_g values of both matrix and composite confirms that nanoparticles did not alter the interactions present at least as regards the amorphous phase of BA.

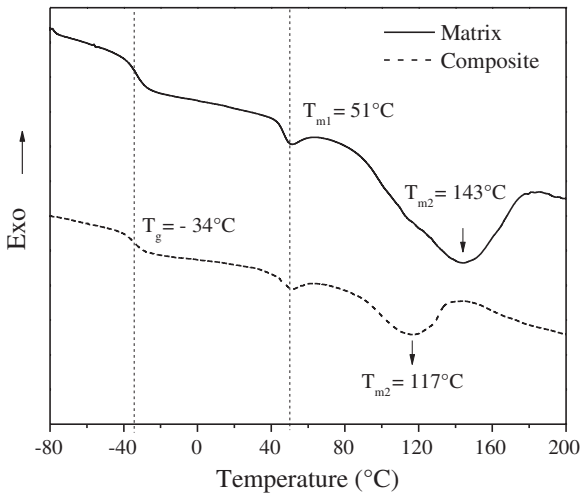

Figure 6. DSC thermograms of matrix and composite.

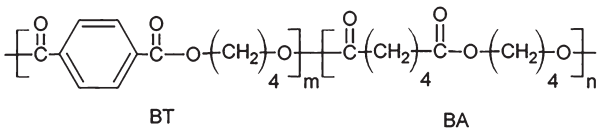

Figure 7. Chemical structure of PBAT. BT, rigid segment; BA, soft segment.

The other two peaks observed in DSC curves represent the melting temperatures, T_{m1} and T_{m2}, associated with the crystal structure of PBAT formed by mixed crystallization of the BT and BA units, respectively.[41] The endothermic peak T_{m1} is related to the formation of a crystal lattice containing mainly BA units, while T_{m2} corresponds to the fusion of crystals related to the stiffer segment of PBAT, BT. The addition of nanoparticles did not modify T_{m1} but shifted T_{m2} towards lower temperatures (by *ca* 26 °C). Nanoparticles can promote the formation of largely imperfect crystals of this segment, which melt at lower temperatures than the PBAT crystals. Besides, it is also possible that the nanoparticle network had imposed a confinement effect on polymer chain diffusion and crystal growth, slowing down the crystallization.[42–44]

Mechanical properties

Figure 8 shows the loss tangent (tan δ) dependence on temperature for the developed films. One very soft and two well-marked peaks can be observed. All peak values are reported in Table 2. The first transition, which corresponds to the glass transition temperature of the flexible segment of PBAT (BA) (T_1),[35] is at *ca* − 32 °C for both matrix and composite but decreases in intensity when nanoparticles are present. The effect of nanoparticles to break starch grains led to an increase of the interfacial area due to the smaller grain size, and hence the intensity of internal frictions involved in this transition increases.

The wide transition, with low intensity, observed at *ca* 50 °C is associated with the starch-rich phase transition (T_2).[4] It shifted slightly to lower temperatures with the addition of nanoparticles. This behaviour is due to the nanoparticle contribution to starch gelatinization during extrusion (as shown by SEM and DTA); thus, there may be more water (Table 1) and glycerol content in the composite in the starch-rich phase compared to the matrix. The approach of the starch transition to the soft phase of PBAT further agrees with the idea that nanoparticles help to improve starch compatibility with PBAT.

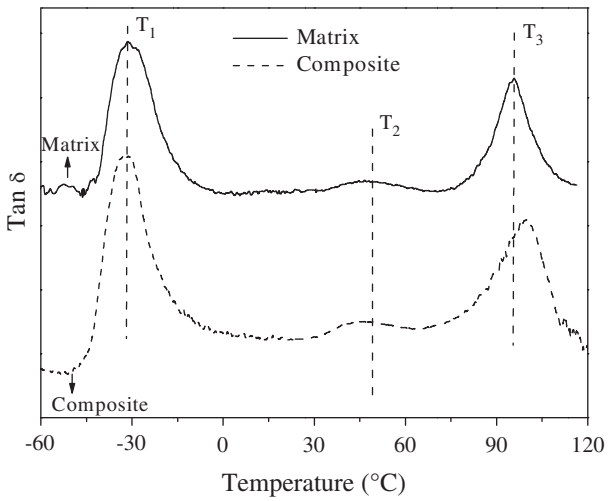

Figure 8. Loss tangent of matrix and composite films as a function of temperature.

Table 2. Uniaxial tensile and dynamic mechanical parameter values of the developed films

	E' (MPa)	σ (MPa)	ε (%)	T_1 (°C)	T_2 (°C)	T_3 (°C)
Matrix	65 ± 5	9 ± 1[a]	295 ± 19[b]	−32 ± 1[c]	−49 ± 1	96 ± 1
Composite	79 ± 6	11 ± 1[a]	284 ± 12[b]	−32 ± 1[c]	−46 ± 1	100 ± 1

[a,b,c] Similar letters in the same column indicate non-significant differences ($P \leq 0.05$).

The last transition observed in the tan δ curves is related to the stiffer segment of PBAT (BT) (T_3).[35] In the composite, it was slightly shifted to higher temperatures and widened compared to that of the matrix. Considering that nanoparticles influenced the fusion of crystals of BT, as described in the DSC assays, it was expected that it also affected the amorphous part of this structure.

Considering together the results of DSC and dynamic mechanical thermal analysis, it can be inferred that the nanoparticles, beyond the interaction with the starch amylose, modified the PBAT rigid segment.

Table 2 also shows the results of the uniaxial tensile parameters. Young's modulus (E), stress at break (σ_b) and strain at break (ε_b) values of the matrix are around 65 MPa, 9 MPa and 295%, respectively. In accordance with the literature, the E of virgin PBAT is around 80 MPa, with a strain at break (ε_b) higher than 600% and stress at break between 15 MPa and 20 MPa.[23,42,45] Using 30 wt% of starch, all uniaxial tensile parameters exhibit slight decreases. This is probably due to the presence of some whole starch grains in the material before the extrusion process (Fig. 1(b)). Starch grains in the matrix can provoke two different effects. On the one hand, starch grains can act as reinforcement and, on the other hand, they can propagate fissures making the interaction between the carbonyl group of the PBAT matrix and the starch with the matrix polymer worse.[17] The reported values of Young's modulus and stress at break in the matrix are similar to those obtained in the literature[17,36,45] when PBAT/starch blends (70:30) were evaluated.

With the addition of nanoparticles, a tendency to increased E and σ_b with a slight decrease in the strain at break was observed. Two factors may be occurring: first, whole starch grains observed in the matrix broke down in the composite reducing the particulate size

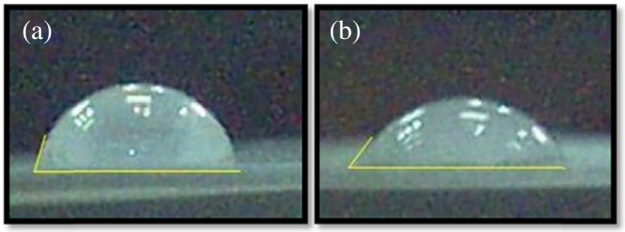

Figure 9. Contact angle of (a) matrix and (b) composite.

of TPS within the biodegradable blend matrix (Fig. 1(c)), leading to an improvement in the plasticization of starch; on the other hand, as can be seen in DSC, the interaction of nanoparticles with the matrix resulted in a reduction in the segmental chain mobility, thereby contributing to higher modulus.[17] Increments in Young's modulus and stress at break are also observed in PBAT/starch blends with the addition of other nanoparticles.[36] Nayak[36] investigated the effect of various weight percentages of clay on a PBAT/starch blend. He demonstrated that 3 wt% of filler improves the mechanical properties. He also explained the mechanical results by the effect of the filler in the reduction of TPS size grains. Olivato *et al.*[15] incorporated 3 wt% of sepiolite in similar PBAT/starch matrices and observed an increase in both Young's modulus and stress at break while maintaining the values of strain at break of the matrix.

The slight increases in modulus and stress at break and the decrease in strain at break in the composite show the two possible effects of the use of nanoparticles: besides the importance of the addition of nanoparticles to help compatibility between starch and PBAT, the nanoparticles contribute to reinforcing the material.

Contact angle

In order to evaluate the hydrophobicity of the films, the contact angle (θ) between a drop of distilled water (2 μL) and the surface of each system was tested (Fig. 9 and Table 1). The incorporation of nanoparticles provoked a decrease in the contact angle for the composite of *ca* 20%, leading to a more hydrophilic material. This behaviour was expected taking into account the hydrophilicity of the starch nanoparticles that leads the composite to a more advanced stage of the gelatinization process (SEM, DTA and FTIR results). The presence of nanoparticles led to a more gelatinized material (SEM and DTA) and an increased number of free carbonyl groups as a consequence of the new interaction pattern present in the PBAT/TPS composite as a result of the interactions between starch and nanoparticles.

The higher hydrophilicity in the composite is consistent with the increase of the value of its water content (Table 1).

Biodegradation of the films in vegetable compost

Figure 10 shows the macroscopic appearance of the films as a function of the time of burial in vegetable compost. The composite showed faster deterioration than the matrix in the evaluated time, indicating that the incorporation of starch nanoparticles improved the biodegradability of the PBAT/TPS films. As can be seen, on the sixth day of storage the composite experienced slight changes in its tonality, in addition to breakdowns, showing the beginning of degradation. This result agrees with that obtained using montmorillonite (hydrophilic nanoclay) as filler in PBAT composites[26] and in PBAT/TPS composites.[23]

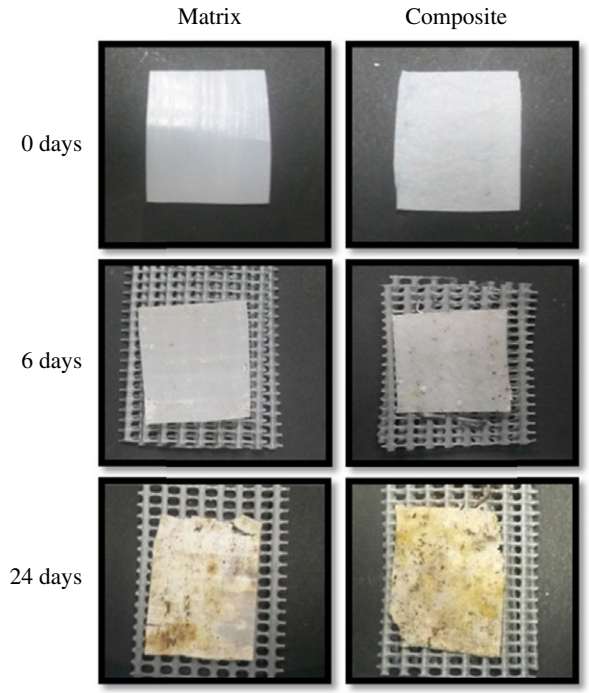

Figure 10. Macroscopic appearance of biodegradation in soil of matrix and composite.

In soil, water diffuses into the polymer sample causing swelling and enhancing biodegradation due to increases in microbial growths. As can be seen in Table 1, the incorporation of nanoparticles increased the moisture content of the films, which led to increases in the chance of microorganism attack. Finally, the decomposition of both matrix and composites occurs more markedly after 24 days of burial.

The faster biodegradability of the composite makes it very interesting as a promising material in line with the new trends in environmental care.

CONCLUSIONS

PBAT/TPS films containing 0.6 wt% of starch nanoparticles have been successfully produced using a twin-screw extruder. The addition of nanoparticles strongly modified the morphology of the PBAT/TPS blend. In the composite, there was a decrease in the number and size of starch grains due to the improvement in material processability, suggesting that nanoparticles led to a higher degree of starch gelatinization. A slight improvement in the compatibility of the components of the system was reached, as shown by the shift in the relaxation of the soft component of PBAT (AT) (T_2) towards the relaxation of starch (T_1).

The incorporation of nanoparticles also changed the interactions present, as well as the structure of the PBAT/TPS film. Nanoparticles interacted by hydrogen bonds with starch amylose and modified the structure of the rigid segment of PBAT (BT). Nanoparticles led to a sharp decrease in the BT melting temperature (T_{m2}) due to a more imperfect structure, as a consequence of the presence of the nanofiller. Nanoparticles also provoked a slight shift towards higher temperatures of the glass transition associated with the amorphous part of the BT segment (T_3).

Interestingly, only 0.6 wt% of nanoparticles modified the mechanical response of the blend. The composite shows increases

of 20% in both Young's modulus and the stress at break, without significant decreases in the strain at break, showing a reinforcing effect of starch nanoparticles in the PBAT/starch blend.

Finally, it is interesting to note that the addition of nanoparticles accelerated the degradation process of PBAT/TPS films, making this composite very interesting as a promising material in line with the new trends in environmental care.

REFERENCES

1 Costa SS, Druzian JI, Machado BAS, Souza CO and Guimarães AG, *Plos One* **9**:12554 (2014).
2 Chen GQ and Martin KP, *Chem Rev* **112**:2082–2099 (2012).
3 Silva JBA, Pereira FV and Druzian JI, *J Food Sci* **77**:N14–N19 (2012).
4 Famá L, Rojo PG, Bernal C and Goyanes S, *Carbohydr Polym* **87**:1989–1993 (2012).
5 Brandelero RPH, Grossmann MV and Yamashita F, *Carbohydr Polym* **90**:1452–1460 (2012).
6 Wang H, Dafu W, Zheng A and Xiao H, *Polym Degrad Stab* **116**:14–22 (2015).
7 Weng YX, Jin YJ, Meng QY, Wang L, Zhang M and Wang YZ, *Polym Test* **32**:918–926 (2013).
8 Torres FG, Troncoso OP, Torres C, Díaz DA and Amaya E, *Int J Biol Macromol* **48**:603–606 (2011).
9 Arruda LC, Magaton M, Suman Bretas RE and Massayoshi Ueki M, *Polym Test* **43**:27–37 (2015).
10 Ren J, Fu H, Ren T and Yuan W, *Carbohydr Polym* **77**:576–582 (2009).
11 Shirai MA, Olivato JB, Salomão Garcia P, Müller CMO, Grossmann MVE and Yamashita F, *Mater Sci Eng C* **33**:4112–4117 (2013).
12 Seligra PG, Medina Jaramillo C, Famá L and Goyanes S, *Carbohydr Polym* **138**:66–74 (2016).
13 Medina Jaramillo C, González Seligra P, Goyanes S, Bernal C and Famá L, *Starch Stärke* **67**:780–789 (2015).
14 Famá L, Bittante AM, Sobral PJA, Goyanes S and Gerschenson LN, *Mater Sci Eng C* **30**:853–859 (2010).
15 Olivato JB, Marini J, Pollet E, Yamashita F, Grossmann MVE and Avérous L, *Carbohydr Polym* **118**:250–256 (2015).
16 Kalambur S and Rizvi SSH, *J Plast Film Sheeting*, **22**:39–58 (2006).
17 Mohanty S and Nayak SK, *Int J Plast Technol* **13**:163–185 (2009).
18 Wei D, Wang H, Xiao H, Zhenga A and Yang Y, *Carbohydr Polym* **123**:275–283 (2015).
19 Le Corre D and Angellier-Coussy H, *React Funct Polym* **85**:97–120 (2014).
20 Salomão Garcia P, Grossmann MVE, Shirai MA, Lazaretti MM, Yamashita F, Mullera CMO *et al.*, *Ind Crop Prod* **52**:305–312 (2014).
21 Olivato JB, Grossmann MVE, Yamashita F, Eiras D and Pessan LA, *Carbohydr Polym* **87**:2614–2618 (2012).
22 Martins AB and Santana RMC, *Carbohydr Polym* **135**:79–85 (2016).
23 Someya N, Kondo N and Shibata M, *J Appl Polym Sci* **106**:730–736 (2007).
24 Angellier H, Molina-Boisseau S, Belgacem MN and Dufresne A, *Langmuir* **21**:2425–2433 (2005).
25 García NL, Ribba L, Dufresne A, Aranguren M and Goyanes S, *Carbohydr Polym* **84**:203–210 (2011).
26 Mohanty S and Nayak SK, *J Polym Environ* **20**:195–207 (2012).
27 Putaux JL, Molina-Boisseau S, Momaur T and Dufresne A, *Biomacromol* **4**:1198–1202 (2003).
28 Condés MC, Añon MC, Mauri AN and Dufresne A, *Food Hydrocolloids* **47**: 146–157 (2015).
29 Yu Y and Wang J, *Food Res Int* **40**:297–303 (2007).
30 Lamanna M, Morales N, García NL and Goyanes S, *Carbohydr Polym* **90**:90–97 (2013).
31 Silva JBA, Lucas AA, Pereira F, Jose NM, Bretas R, Miranda CS *et al.*. Processo de preparação de blendas poliméricas ambientalmente degradáveis reforçadas com nanocristais/nanowhiskers de celulose para produção de filmes flexíveis por extrusão, No Registro 011120000389, BR Patent INPI 011120000389, BR102012014512-0 (2012).
32 ASTM D882-02, *Annual Book of ASTM*. American Society for Testing and Materials, West Conshohocken, PA (2002).
33 Karbowiak T, Debeaufort F, Champion D and Voilley A, *J Colloid Interface Sci* **294**:400–410 (2006).
34 AOAC, *Official Methods of Analysis*. Association of Official Analytical Chemists, Washington, DC (1995).
35 Olivato JB, Grossmann MVE, Bilck AP and Yamashita F, *Carbohydr Polym* **90**:159–164 (2012).
36 Nayak SK, *Polym Plast Tech Eng* **49**:1406–1418 (2010).
37 Garcia NL, Ribba, L, Dufresne A, Aranguren MI and Goyanes S, *Macromol Mater Eng* **294**:169–177 (2009).
38 Kijchavengkul T, Auras R and Rubino M, *Polym Test* **27**:55–60 (2008).
39 Chiangga S, Suwannasopon S and Trivijitkasem NS, *Kasetsart J (Nat Sci)* **47**: 781–789 (2013).
40 García NL, Famá L, Dufresne A, Aranguren M and Goyanes S, *Food Res Int* **42**:976–982 (2009).
41 Al-Itry R, Lamnawa K, Maazouz A, Billon N and Combeaud C, *Eur Polym J* **68**:288–301 (2015).
42 Fukushima K, Wu MH, Bocchini S, Rasyida A and Yang MC, *Mater Sci Eng C* **32**:1331–1351 (2012).
43 García NL, Lamanna M, D'Accorso N, Dufresne A, Aranguren M and Goyanes S, *Polym Degrad Stab* **97**:2021–2026 (2012).
44 Morales NJ, Candal R, Famá L, Goyanes S and Rubiolo GH, *Carbohydr Polym* **127**:291–299 (2015).
45 Stagner J, Dias Alves V and Narayan R, *J Appl Polym Sci* **126**:E135–E142 (2012).

